Geometrical Investigation of a U-shaped Oscillating Water Column Wave Energy Device

De-zhi Ning [a], Bao-ming Guo [a], Rong-quan Wang [a,*], Thomas Vyzikas [b], Deborah Greaves[b]

[a] State Key Laboratory of Coastal and Offshore Engineering, Dalian University of Technology, Dalian, 116024, China

[b] School of Engineering, Computing and Mathematics, University of Plymouth, Drake Circus, PL48AA, Plymouth, UK

Abstract: Hydrodynamic performance of a fixed U-shaped Oscillating Water Column (U-OWC) Wave Energy Converter is numerically investigated. Based on the time-domain higher-order boundary element method (HOBEM), a two-dimensional fully nonlinear numerical model is implemented to simulate the nonlinear wave interaction with a U-OWC device. In the model, the inner-domain-source method is adopted to generate the incident waves and a linear pneumatic model is used to determine the air pressure which is imposed on the free surface inside the chamber. The numerical model is well validated against the published experimental data of the free surface elevation at the chamber center, air pressure inside the chamber and hydrodynamic efficiency. Further, the present model is applied to study the effects of geometrical parameters (including the vertical duct height, vertical duct width and wall thickness) on the hydrodynamic performances of the U-OWC device. The results indicate that geometrical parameters of the vertical duct have significant influence on the air pressure inside the chamber and the hydrodynamic efficiency. The hydrodynamic efficiency and air pressure inside the chamber are found to increase with the increase of both vertical duct height and thickness of wall I. However, the increasing rate of the efficiency slows down gradually with the thickness of wall I increasing, which indicates that a comprehensive consideration of the construction cost and hydrodynamic performance

---

* Corresponding author. E-mail: rqwang@dlut.edu.cn

is needed in the design and construction of a U-OWC device.

1. Introduction

Energy supply and climate change have plagued human society for decades. Hence, it is significant for human being to exploit the clean renewable energies. In this regard, ocean energies have attracted a large amount of attention because of their viable alternative [1]. Amongst those, wave energy exhibits greater potentiality than other ocean energies due to its high energy flux density and constructive hydrodynamic interaction of multi-converters.

A great deal of research on wave energy converters (WECs) has been carried out. Therein, the Oscillating Water Column (OWC) WEC appears to be one of the most successful and the ripest types. The OWC-WECs were investigated theoretically, experimentally and numerically by Evans and Porter [2], Martins-rivas and Mei [3], Zheng et al. [4] Deng et al. [5], Ning et al. [6], Wang and Ning [7], and so on. In recent years, the floating OWC-WECs were proposed to expand the application area of the OWC devices, such as Falcão et al. [8], Gomes et al. [9], Crespo et al. [10], He and Huang [11]. Furthermore, The OWC-WECs with dual chambers were investigated by Rezanejad et al. [12], He et al. [13], Ning et al. [14, 15], etc., which can broaden the effective frequency bandwidth by inducing more resonant frequencies of the device. Not only various types are proposed, but also the geometrical design details are investigated to further improve the performance and survivability of OWC devices. For instance, the effects of front wall draft, slope degree of front wall and chamber width on the hydrodynamic performance of the OWC devices were investigated in [16-18]. Based on those crucial researches, prototypes of the OWC-WECs have also been built in several countries [19-21].

A variant OWC device was proposed by Boccotti [22], named as U-shaped oscillating water column (U-OWC) device, consisting of an air chamber, a Power Take-

Off (PTO) system, which often simulated by an orifice located at the air chamber celling, and an additional vertical duct as shown in Fig. 1. The vertical duct changes significantly the excitation form of the U-OWC device with respect to the conventional OWC device. The incident wave trains cannot propagate into the inner chamber, but the hydrodynamic force exerted at the upper opening of the vertical duct induces an up and down motion of the water column and then a reciprocating air-flow through the orifice. Compared to the conventional OWC device, the eigenperiod of the U-OWC device and the air pressure inside the U-OWC chamber are larger [22]. Additionally, the U-OWC device can avoid sand entering into the chamber and can also decrease air inhalation at bottom opening, which benefits the security of the device.
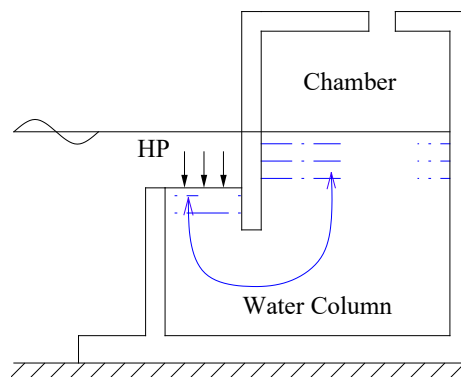
Figure 1 A schematic of the U-OWC device.

Hydrodynamic investigations on the U-OWC device have been carried out theoretically, numerically and experimentally since its concept was put forward. Initially, Boccotti [23] proposed the concept of the U-OWC device and pointed out its advantages. Successively, the related theoretical derivations and numerical simulations were performed. One theoretical framework of inner water column oscillation was introduced by Boccotti [24] according to the unsteady Bernoulli theorem. Later, Boccotti et al. [25] performed a laboratory experiment to validate the reliability of the theoretical model. Malara and Arena [26] developed a numerical model by coupling the eigenfunction expansion method outside the U-OWC device based on linear wave

theory with the unsteady Bernoulli equation in the internal region. Malara et al. [27] revised the underrated head losses in the previous theoretical model. They introduced the unsteady head losses into motion equation based on the acceleration-based technique and implemented a field experiment to calibrate it. Soon afterwards, Malara et al. [28] developed a three-dimensional (3D) numerical model of the U-OWC device based on the boundary integral equations method in the frequency domain and linear wave theory. Spanos et al. [29] employed a statistical linearization method to describe the motion of the U-OWC. Malara and Arena [30] proposed a semi-analytical approach to calculate the hydrodynamic efficiency of the U-OWC WEC array. They found that the array reduces the hydrodynamic efficiency of the U-OWC device with respect to the isolated U-OWC device. Strati et al. [31] adopted the Maximum Power Point Tracking (MPPT) algorithm to control the coupling between the U-OWC device and the PTO system. Some experiments were also conducted in addition to the above numerical models. Vyzikas et al. [32] experimentally studied the hydrodynamic performance of four variants of a three-chamber OWC model with and without the PTO system. The experimental data indicated that the hydrodynamic efficiency of the U-OWC device is superior to the traditional OWC device, especially for the U-OWC device with a bottom slope. Arena et al. [33] conducted a field experiment to analyze the interaction between the Dielectric Elastomer Generator (DEG) PTO system and the U-OWC device. From the engineering perspective, Boccotti [34] explored some regulations to guide the overall design of the full-scale U-OWC WEC. Arena et al. [35] discussed the crucial issues on the design and construction stages of the U-OWC device. Monte Carlo simulation was utilized to determine the inner free surface displacement and the maximum load exerting on the walls, and further to evaluate the working condition of the PTO system and the safety of the air chamber.

Most of the previous studies were mainly focused on the theoretical models and investigating the effects of the PTO system on the hydrodynamic efficiency. There is a lack of investigation on the influence of the geometrical parameters on the

hydrodynamic performance of the U-OWC device. Moreover, the theoretical studies of the U-OWC device were mostly based on linear wave theory. However, the hydrodynamics of the wave interaction with U-OWC device is quite complicated and nonlinear. In the present study, based on the fully nonlinear potential flow theory and higher-order boundary element method (HOBEM), the effects of the geometrical parameters (i.e., the vertical duct height, vertical duct width and barrier wall thickness) on the hydrodynamic performance of a U-OWC device are numerically investigated.

The rest of the present paper is organized as follows. The numerical model is described in section 2. Reliability and accuracy of the model are verified in section 3. Effects of geometrical parameters on the hydrodynamic performance of the U-OWC device are investigated in section 4. Finally, conclusions are summarized in Section 5.

2. Numerical model

The two-dimensional (2-D) fully nonlinear numerical wave flume based on the time-domain HOBEM developed by Ning et al. [36] to investigate the hydrodynamic performance of an OWC device is extended here to simulate the wave interaction with the U-OWC device. In the numerical model, an inner-source technique is adopted to generate the incident wave so that the re-reflection on the input boundary of the numerical wave flume (NWF) can be avoided. Meanwhile, a pneumatic model is used to determine the air pressure which is imposed on the free surface inside the chamber.

A schematic diagram of the NWF with a U-OWC wave energy converter is shown in Fig. 2. Herein, a Cartesian coordinate system is set up with its origin (O) at the intersection point of inner-source surface and undisturbed free surface, x-axis positive in the direction of incident wave propagation, and z-axis positive upwards. As shown in Fig. 2, h is the still water depth; a is the orifice width; b, c_I, c_II, e and l are the air chamber width, thickness of barrier wall I, thickness of barrier wall II, vertical duct width and base length (before the vertical duct), respectively; d, w and s are the draught of barrier wall II, vertical duct height and base height, respectively.
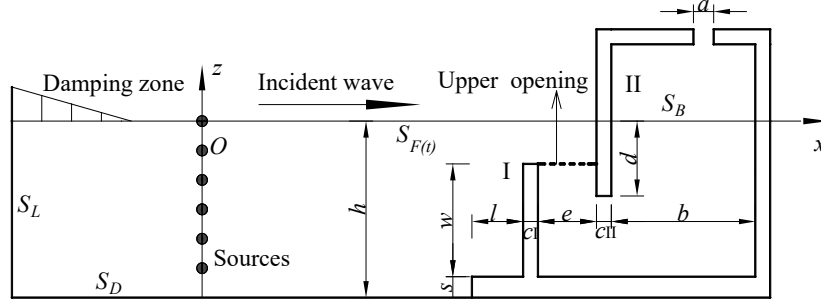
1

2   Figure 2 Schematic diagram of a U-OWC device in the numerical flume.

3

4   The assumptions of inviscid, incompressible and irrotational flow are usually used

5 in the wave-OWC simulation and good accuracy is achieved [36-38]. Thus, the

6 simulation of the present study about the wave- U-OWC interaction can also be

7 described by potential theory, where velocity potential ϕ satisfies Laplace equation in

8 the computational domain. Therein, due to the introduction of inner sources, Laplace

9 equation was altered into Poisson equation as follows:

10

$$\nabla^2\phi = q^*\left(z,t\right) = 2v\delta\left(x\right) \qquad \text{in} \quad \Omega \tag{1}$$

11 in which $\nabla^2 = \partial^2/\partial x^2 + \partial^2/\partial z^2$ is the 2-D Laplacian operator, and $q^*(z,\ t)$ is the

12 pulsating volume flux density of the internal sources (the horizontal position of vertical

13 sources is located at $x=0$), v the horizontal fluid velocity given by Stokes second-order

14 analytical solution in the present study, which denotes the sources strength, $\delta(x)$ is the

15 Dirac delta function, and Ω denotes the whole fluid domain, which is surrounded by the

16 instantaneous free surface $S_{F(t)}$, the flume bottom S_D, the left boundary S_L and the

17 surface of the U-OWC device S_B as shown in Fig. 2.

18   On the instantaneous free surface, an artificial damping coefficient is involved in

19 the dynamic free surface boundary condition inside the chamber to consider the head

20 losses due to the flow separation and vortex shedding caused by barrier wall I and II.

21 The mixed Eulerian-Lagrangian method is employed to describe the instantaneous free

22 surface with moving nodes in both x and z directions. A damping zone at the left

23 boundary of the NWF is adopted to eliminate reflected waves from the U-OWC device.

1   Thus, the kinetic and dynamic boundary condition can be rewritten as follows:

2
$$\begin{cases} \dfrac{\mathrm{d}X(x,z)}{\mathrm{d}t} = \nabla\phi - \mu_1(x)(X - X_0) \\ \dfrac{\mathrm{d}\phi}{\mathrm{d}t} = -g\eta - \dfrac{P}{\rho} + \dfrac{1}{2}|\nabla\phi|^2 - \mu_1(x)\phi - \mu_2(x)\dfrac{\partial\phi}{\partial n} \end{cases} \quad \text{on} \;\; S_{F(t)} \qquad (2)$$

3   where $\mathrm{d}/\mathrm{d}t = \partial/\partial t + V\cdot\nabla$ is the material derivative, V the velocity of water particle,

4    $X(x, z)$ the horizontal and vertical displacements of fluid particles on the free surface, t

5   the time, η the free-surface elevation, P the air pressure inside the chamber caused by

6   the oscillating motion of the water column, and $\mu_1(x)$ is the damping layer coefficient,

7   X_0 the initial position of fluid particles, g the gravity acceleration, ρ the fluid density.

8    $\mu_2(x)$ denotes the artificial damping coefficient. $\mu_1(x)$ and $\mu_2(x)$ can be defined as follows:

9
$$\mu_1(x) = \begin{cases} \omega\left(\dfrac{x - x_1}{L}\right)^2, & x_1 - L < x < x_1 \\ 0, & x \geq x_1 \end{cases} \qquad (3)$$

10
$$\mu_2(x) = \begin{cases} \text{confirmation} & \text{inside of the chamber} \\ 0 & \text{outside of the chamber} \end{cases} \qquad (4)$$

11   where ω denotes the angular frequency of the incident wave, L the length of the

12   damping layer, x_1 the starting position of the damping zone, and 'confirmation' means

13   that the specific value need to be determined by the trial-and-error method [6].

14   It is assumed that the flume bottom S_D, left boundary S_L and body surface S_B are

15   the impermeable fixed boundary, and the fluid never separates from those boundaries.

16   Thus, the water particle speed is equal to 0 in its normal direction.

17
$$\frac{\partial\phi}{\partial \boldsymbol{n}} = 0 \;\; \text{on} \;\; S_D, S_L \;\text{and}\; S_B \qquad (5)$$

18   where $\boldsymbol{n}$ is the outward normal unit vector on those solid boundaries.

19   The above-mentioned problem is not only a boundary value problem, but a time-

20   dependent problem. The initial condition should be given to solve aforementioned

21   equations in time domain.

22
$$\begin{cases} \phi|_{t=0} = 0 \\ \eta|_{t=0} = 0 \end{cases} \quad \text{on} \;\; S_{F(t)} \qquad (6)$$

There is a strong coupling between the air and water inside the U-OWC chamber because the air pressure is directly related to the oscillation of the free-surface inside the chamber. The numerical model assumes a linear relationship between the air pressure and the air flow velocity through the duct. The air pressure inside the chamber can be expressed as follows:

$$P(t) = C_{dm} U_d(t) \tag{7}$$

where C_{dm} denotes the linear pneumatic damping coefficient and U_d the air flow velocity at the orifice. Due to small-scale simulation considered, the air inside the chamber is assumed to be incompressible [14]. The detail information about the pneumatic model can be found in [36].

The above boundary value problem can be solved by HOBEM. Herein, to avoid the numerical instabilities, the free surface is re-meshed and updated at each time step and the quadratic shape function interpolation is adopted to compute the velocity potential and spatial position of new nodes. The more details about the HOBEM can be referred to [36].

The hydrodynamic efficiency is defined as a rate of the captured energy against the incident wave energy per unit width. The average captured energy by the U-OWC device during one period can be calculated by

$$P_{cap} = \frac{1}{T} \int_t^{T+t} Q(t) P(t) dt = \frac{1}{T} \int_t^{T+t} b\bar{\bar{\eta}}(t) P(t) dt = \frac{1}{T} \int_t^{T+t} aU_d(t) C_{dm} U_d(t) dt \tag{8}$$

where T is the wave period, $Q(t) = b\bar{\bar{\eta}}(t) = aU_d(t)$ is the airflow rate through the orifice and $\bar{\bar{\eta}}(t)$ is the time-dependent mean vertical velocity of the free surface inside the chamber.

Based on the incident wave conditions, the wave nonlinearity is weak. Thus, the incident average energy flux per unit width can be calculated based on the linear wave theory:

$$P_{inc} = \frac{1}{2} \rho g A^2 C_g \tag{9}$$

where A is the incident wave amplitude, $C_g = d\omega/dk$ the wave group velocity, k the wave number. The hydrodynamic efficiency can be calculated as:

$$C_w = P_{cap} / P_{inc} \tag{10}$$

3. Model validation

In this section, the U-OWC numerical model is validated by comparing with the published experimental data [32]. Fig. 3 depicts the experimental setup of the U-OWC device, where locations of pressure gauges, wave gauges and orifices are given. The details of geometrical parameters are listed in Tab. 1. The related geometrical parameters and incident wave parameters in the numerical model are identical with those in the experiment. It's noteworthy that the orifice width in the numerical model is determined by assuming that the opening ratio in the numerical model is equal to that in the experiment. This paper mainly concerns the hydrodynamic performance of the U-OWC device subjected to regular incident waves. The incident wave frequencies are 0.57, 0.51, 0.465 and 0.385 Hz corresponding to wave heights of 0.122, 0.096, 0.088 and 0.159 m, respectively. The damping coefficient $\mu_2 = 0$ and the pneumatic damping coefficient $C_{dm} = 19$ kg/ (m^2·s) are adopted by the trial and error method [6]. The left damping layer is set as 1.5 times wavelength λ (total length of NWF is 5 times wavelength). The simulation is based on potential theory, so generic personal computer is enough to complete the calculation, where an i7 CPU with six cores is used.
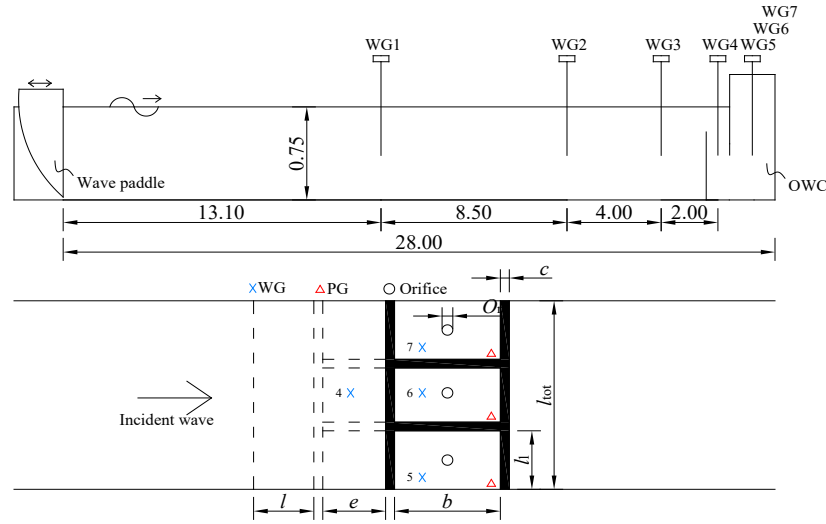
Table 1 Geometrical parameters of U-OWC device (m).

a	b	c_{I}	c_{II}	d

|				
9.6×10^{-4}	0.286	0.024	0.024	0.482
e	l	w	s	h
0.143	0.143	0.447	0.107	0.750

1

2

3   Figure 3 (a) Side view and (b) plan view of the U-OWC experimental model Vyzikas et al. [32].

4

5   The additional vertical duct influences greatly the hydrodynamic performance of

6   the U-OWC device, thus it is necessary to re-verify the convergence of temporal and

7   spatial discretization. Fig. 4 illustrates the time histories of the free-surface elevation at

8   the chamber center and air pressure inside the chamber for three spatial steps of $\triangle x=$

9    $\lambda/20$, $\lambda/30$ and $\lambda/40$ (where λ is the wavelength) with $f = 0.51$ Hz and temporal step $\triangle t=$

10   $T/60$. Similar tests are carried out for three temporal steps of $\triangle t= T/40$, $T/60$ and $T/80$

11   as depicted in Fig. 5, where $f= 0.51$ Hz and spatial step $\triangle x= \lambda/30$. It should be noted

12   that, due to the spatial step varying with the wavelength, meshes near the U-OWC

13   device is refined to ensure the accuracy and stability of the simulation. From the figures,

14   it can be seen that the results with the intermediate spatial/temporal steps agree well

15   with those with the fine spatial/temporal steps. Finally, the mesh size $\triangle x$ and time step

16   $\triangle t$ are chosen to be $\lambda/30$ and $T/60$, respectively. Additionally, the numerical stability of

17   the model is validated in Fig. 6. It can be seen that the two wave profiles agree well

1 with each other both outside and inside the U-OWC chamber at $t=28T$ and $30T$. This

2 indicates that the present numerical model with inviscid assumption can reproduce the

3 interaction between waves and U-OWC device well. Concurrently, the damping zone

4 shows good wave absorbing ability at the left end of the flume. However, the wave

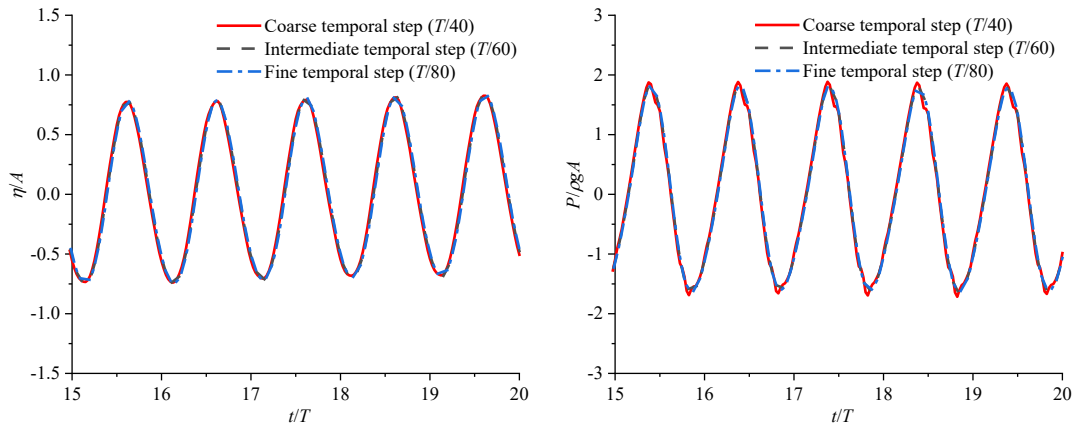5 profile is irregular and higher-order harmonics occur due to the wave nonlinearity.

6
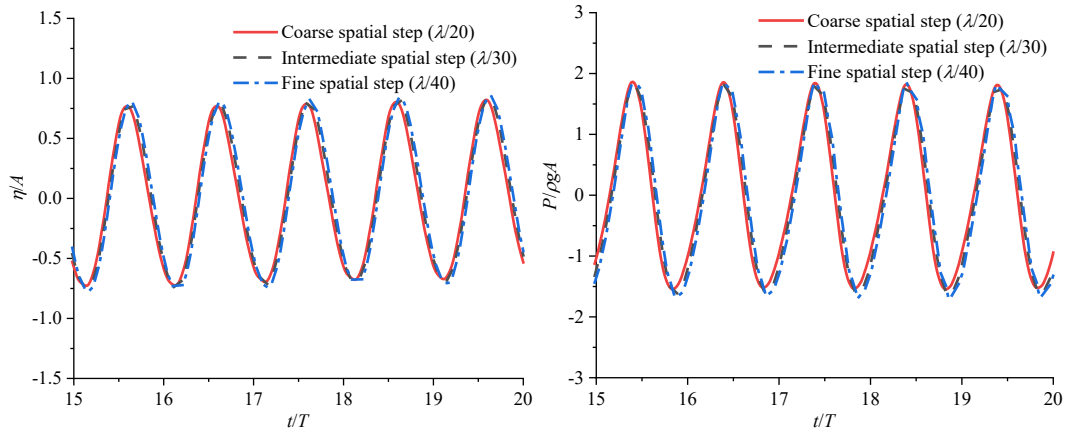
7

8   (a) Surface elevation at the chamber center   (b) Air pressure inside the chamber

9 Figure 4 Time series of surface elevation and air pressure for different spatial steps.

10

11

12   (a) Surface elevation at the chamber center   (b) Air pressure inside the chamber

13 Figure 5 Time series of surface elevation and air pressure for different temporal steps.

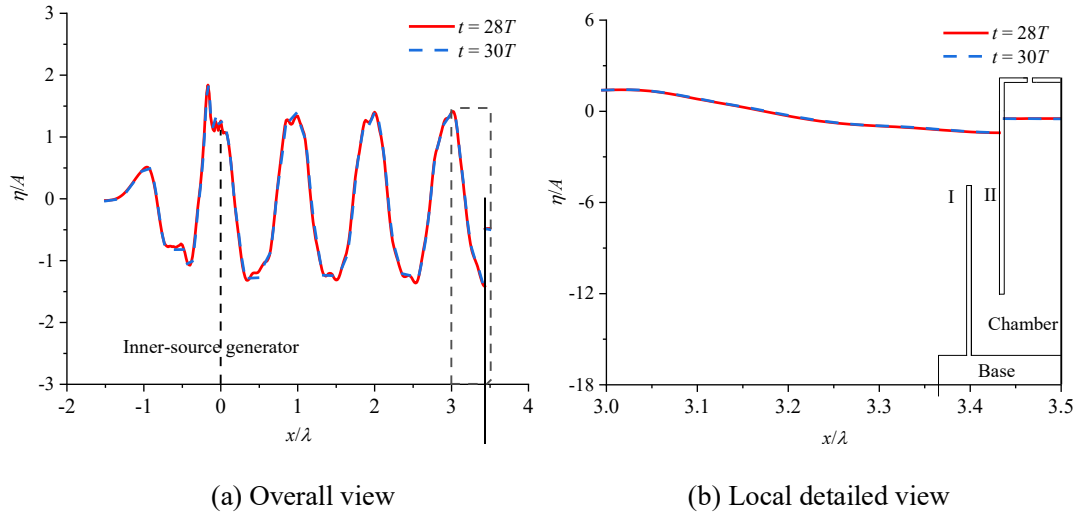(a) Overall view (b) Local detailed view

Figure 6 Snapshot of free-surface elevation along wave flume at f = 0.51 Hz.

Time series of the surface elevation at the chamber center and air pressure in the chamber are depicted for different wave frequencies in Fig. 7 and Fig. 8, respectively. The comparisons between the experiment [32] and the present numerical model are given in the figures. It can be observed that the surface elevation and air pressure predicted by the numerical model agree well with the experimental results. However, due to using linear pneumatic model, the high-order harmonics of the air pressure which occurs in the experimental data are not well predicted.
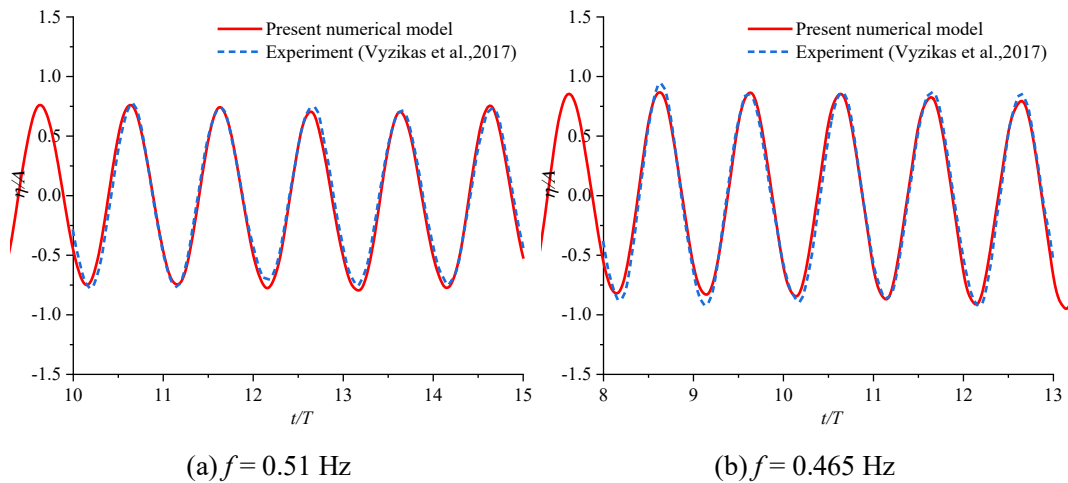

(a) f = 0.51 Hz (b) f = 0.465 Hz

Figure 7 Time series of surface elevation at the chamber center for different wave frequency.

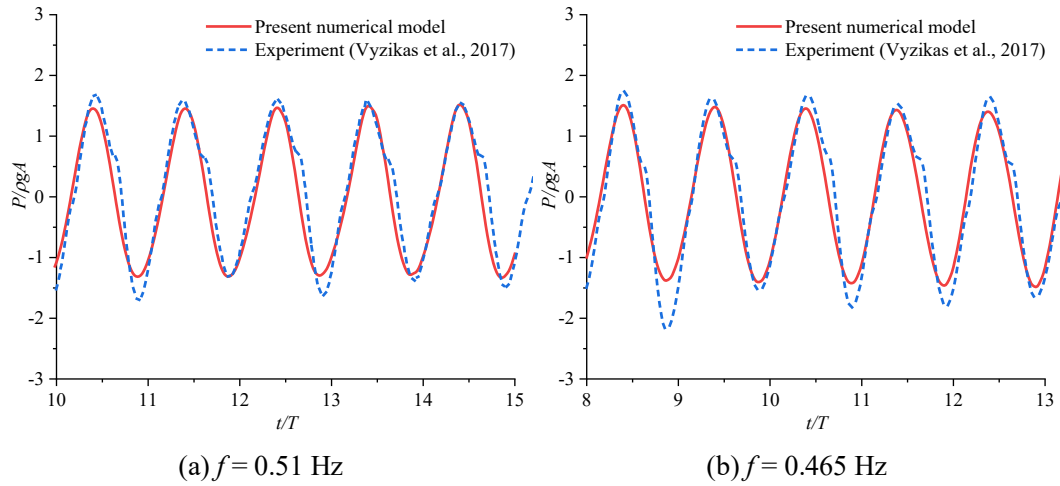(a) $f = 0.51$ Hz   (b) $f = 0.465$ Hz

Figure 8 Time series of air pressure in the chamber for different wave frequency.

Fig. 9 shows the variations of the surface elevation at the chamber center and hydrodynamic efficiency versus wave frequency. It can be seen that the measured and simulated surface elevations and hydrodynamic efficiencies agree well with each other. As a whole, the numerical model can well simulate the main hydrodynamic behaviors of the U-OWC device.
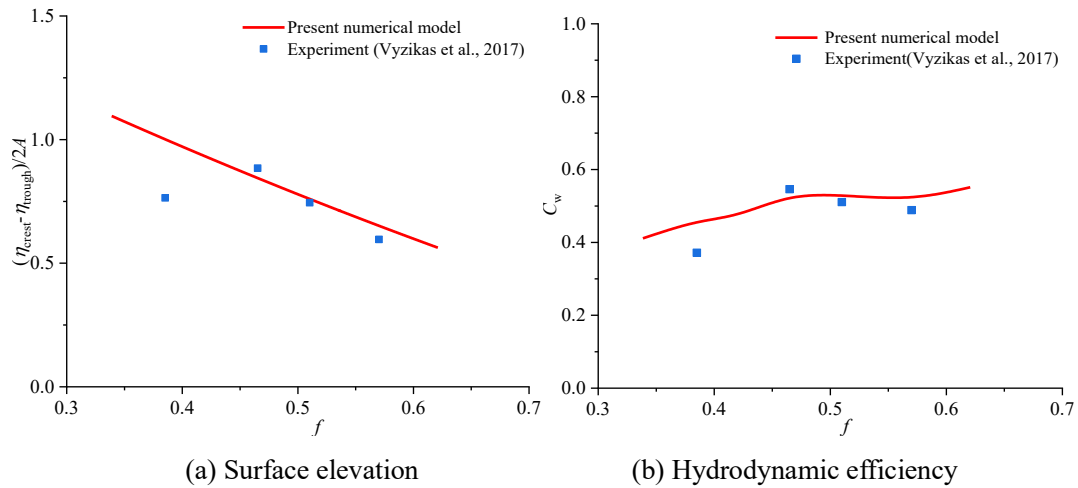

(a) Surface elevation   (b) Hydrodynamic efficiency

Figure 9 (a) Amplitude of surface elevation at the chamber center and (b) hydrodynamic efficiency versus wave frequency.

4. Numerical results and discussions

In this section, the sensibility of some geometrical parameters (i.e., vertical duct

1 height, vertical duct width and thickness of barrier wall I) on the hydrodynamic

2 performance of the U-OWC device are performed. Totally, 78 cases are simulated. The

3 amplitudes of the free-surface elevation at the chamber center and the air pressure inside

4 the chamber are normalized as follows:

$$\eta_{max} = \frac{\left(\eta_{crest} - \eta_{trough}\right)}{2A} \qquad (11)$$

$$P_{max} = \frac{\left(P_{crest} - P_{trough}\right)}{2\rho g A} \qquad (12)$$

7 where η_{max} and P_{max} denote the amplitudes of the free-surface elevation at the chamber

8 center and the air pressure inside the chamber, respectively; η_{crest} and P_{crest} are the mean

9 crest values of the time series of free-surface elevation and air pressure, respectively,

10 η_{trough} and P_{trough} the corresponding mean trough values; A is the incident wave

11 amplitude and is taken as 0.04 m.

4.1 Effect of vertical duct height w

13   To study the effect of the vertical duct height (which is equal to the height of the

14 barrier wall I) on the hydrodynamic performance of the U-OWC device, the numerical

15 simulation is carried out for different vertical duct heights w with other geometrical

16 parameters kept constant as listed in Tab. 1.

17   The variations of the surface-elevation amplitude at the chamber center and the air

18 pressure in the chamber versus dimensionless wavenumber kh for four vertical duct

19 heights $w/h = 0, 0.297, 0.596$ and 0.729 are shown in Fig. 10(a) and (b), respectively.

20 Those symbols denote the original data and their fitting lines. It is found that the free-

21 surface elevation at the chamber center and the air pressure inside the chamber increase

22 with vertical duct height w increasing. This is due to the fact that the distance between

23 the upper opening and water surface decreases with the increase of the vertical-duct

24 height, which leads to the increase of excitation pressure at the upper opening. On the

25 other hand, according to the vertical eigenfunction in linear wave theory, the

26 hydrodynamic pressure decays exponentially along the negative z direction and its

1 decay rate increases with wavenumber kh. This leads to the excitation pressure

2 difference between the tested cases increases with wavenumber kh. Eventually, the

3 effect of the vertical duct height on P_{max} increases with kh increasing in relatively low

4 frequency region (i.e., the difference between any two curves increases with kh

5 increasing as shown in Fig. 10(b)). However, the difference decreases with the further

6 increase of kh due to the increasing wave nonlinearity. In addition, an obvious peak is

7 observed from the air pressure curves at w/h=0.729. This may be due to the shallow

8 water effect for the quite small water depth above the Wall I at this case. Note that, due

9 to the limitation of the water depth, base thickness and incident wave conditions, and

10 the influence of the wave nonlinearity and reflection, the largest vertical duct height w

11 is chosen to be 0.547 m (i.e., $w/h = 0.729$) in the present study.

12

13

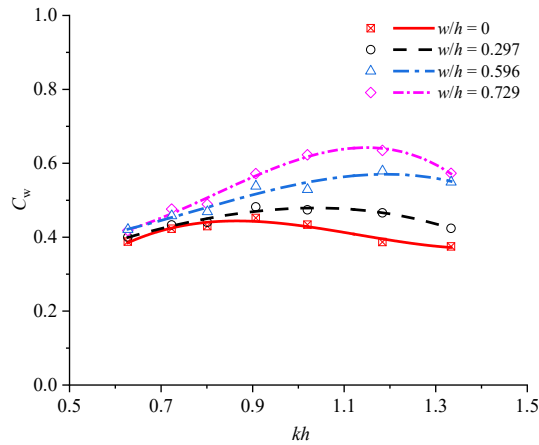14   (a) Surface-elevation   (b) Air pressure
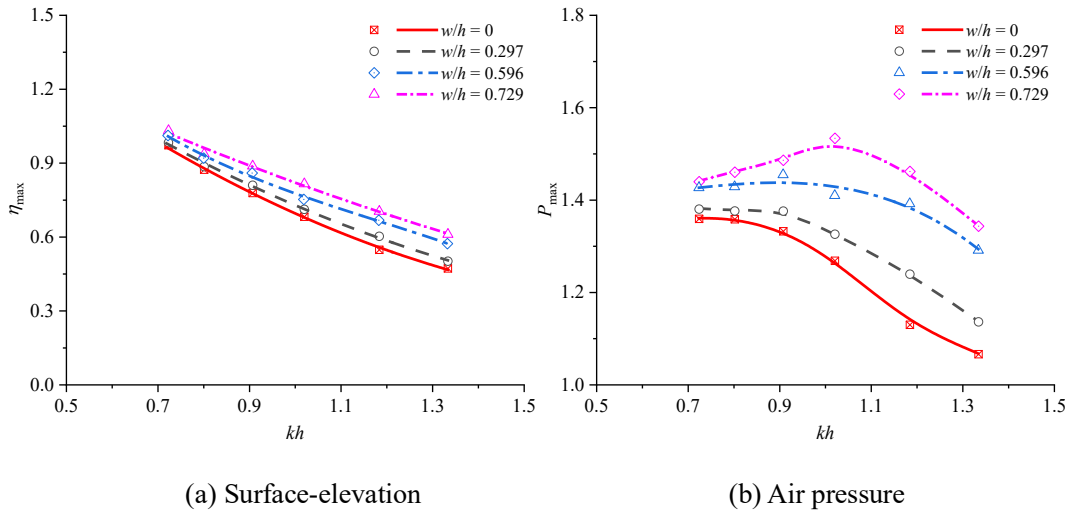
15 Figure 10 Amplitudes of the (a) surface-elevation at chamber center and (b) air pressure inside the

16   chamber versus dimensionless wavenumber kh for different vertical duct heights.

17

18   As discussed above, the vertical duct height has significant influence on air

19 pressure inside the chamber of the U-OWC device. To have a better understand of the

20 influence of the vertical duct on the hydrodynamic performance, Fig. 11 shows the

21 variation of hydrodynamic efficiency versus kh for four vertical duct heights of $w/h =$

22 0, 0.297, 0.596 and 0.729. The cubic fitting lines of the simulated scatter data are also

1 plotted in the Fig. 11. The hydrodynamic efficiency C_w increases with the increase of

2 the vertical duct height w and the effect of the vertical duct height on C_w increase as kh

3 increases in relatively low domain. According to Eq. (8), the hydrodynamic efficiency

4 C_w highly depends on the air pressure inside the chamber. Indeed, the similar

5 phenomenon also emerges on the air pressure inside the chamber as can be seen in Fig.

6 10(b). From Fig. 11, the optimal hydrodynamic efficiencies of 0.44, 0.48, 0.57 and 0.64

7 occur at around kh =0.86 (w/h = 0), kh = 1.03 (w/h = 0.297), kh = 1.18 (w/h = 0.596)

8 and kh=1.14 (w/h = 0.729), respectively. Additionally, one can easily draw a conclusion

9 from Figs. 10 and 11 that the U-OWC device performs better than the conventional

10 OWC device (i.e., the case of w/h = 0) on the power absorption. The similar conclusion

11 was also obtained by Boccotti [22]. He pointed out that the better performance of the

12 U-OWC device is due to the fact that the dynamic pressure exerted at the upper opening

13 of the U-OWC is larger than that at the opening of the conventional OWC device.
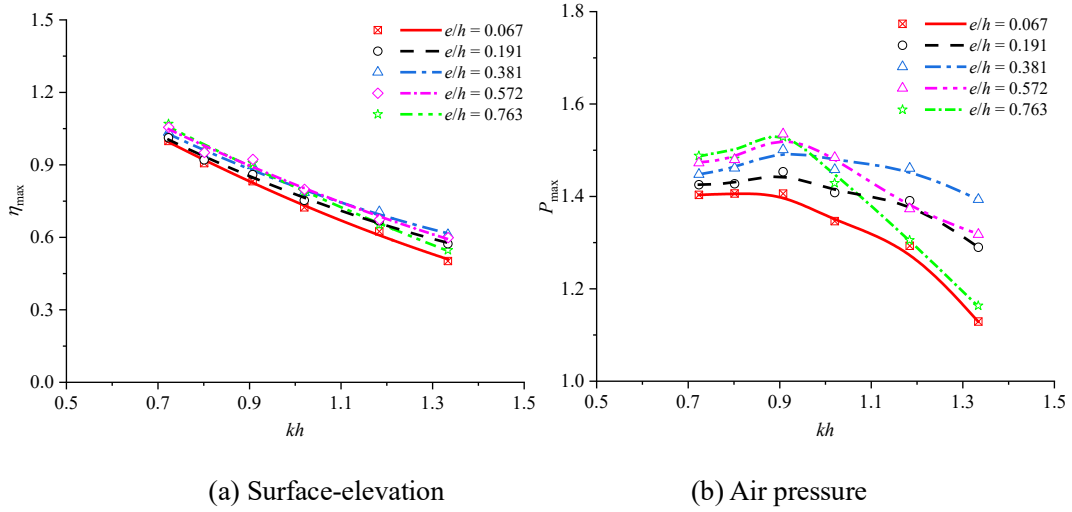
14

16 Figure 11 Hydrodynamic efficiency versus dimensionless wavenumber for different vertical duct

17 heights.

18

19 ## 4.2 Effect of vertical duct width e

20 Fig. 12 shows the free surface-elevation amplitude at the chamber center and the

21 air pressure inside the chamber versus kh for five vertical duct widths of e/h = 0.067,

1   0.191, 0.381, 0.572 and 0.763 with remaining geometrical parameters kept constant as

2   listed in Tab. 1. As shown in Fig. 12(a), the free surface elevation η_{max} is insensitive to

3   the variation of vertical duct width and η_{max} decreases with the increase of kh

4   monotonously. Differently, the vertical duct width has a great influence on the air

5   pressure inside the chamber as shown in Fig. 12(b). Moreover, the surface elevation at

6   the chamber center and the air pressure inside the chamber increase with relative

7   vertical duct width e/h in relatively low frequency region. However, in high frequency

8   region, η_{max} and P_{max} first increase and then decrease with the increase of e/h, and both

9   the increasing and decreasing rates increase with increasing kh.

10

12   (a) Surface-elevation   (b) Air pressure

13   Figure 12 Amplitudes of the (a) surface-elevation at the chamber center and (b) air pressure inside

14   the chamber versus dimensionless wavenumber for different vertical duct widths.

15

16   Fig. 13 shows the variation of hydrodynamic efficiency versus kh for various

17   vertical duct widths. It can be seen that the hydrodynamic efficiency also displays

18   similar variations to air pressure inside the chamber. A proper explanation for such

19   phenomenon is that the hydrodynamic pressure at the upper opening changes little

20   along the x direction because the vertical duct width is small enough compared to the

21   wavelength and wave nonlinearity is relatively small when kh is relatively low. In view

22   of this, the total hydrodynamic force exerted on the U-shaped water column almost

1   increases linearly with the vertical duct width increasing, which strengthens the

2   oscillation of wave column and further leads to the increase of the air pressure inside

3   the chamber. However, the spatial inhomogeneity of the hydrodynamic pressure cannot

4   be ignored with the wavenumber increasing.

5
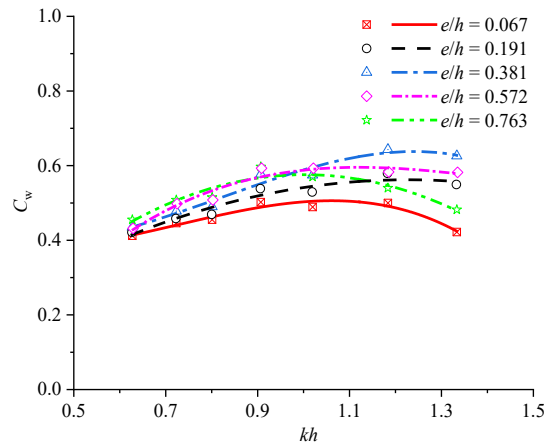
6

7   Figure 13 Hydrodynamic efficiency versus dimensionless wavenumber for different vertical duct

8   widths.

9

10   Fig. 14(a) and (b) show the distribution of the free-surface elevation at the upper

11 opening of the U-OWC device while wave crest arrives at barrier wall II for vertical

12 duct width of e/h= 0.381 and 0.763, respectively. To make the horizontal position of the

13 back wall to be 0, a coordinate translation "x-3.5λ" is used in the Fig. 14. The horizontal

14 inhomogeneity can be clearly observed. It can be seen that the wave-surface slope

15 before the device become steeper with the wave frequency kh increasing from 0.627 to

16 1.184 due to the increase of wave nonlinearity. In other words, the free-surface

17 elevation changes little along x direction near the barrier wall II at kh= 0.627; while it

18 presents great variation along x direction at kh= 1.184, and this phenomenon becomes

19 more obvious with increasing the vertical duct width. Such inhomogeneity of the

20 surface elevation outside the chamber does not benefit the wave energy absorbing.

21

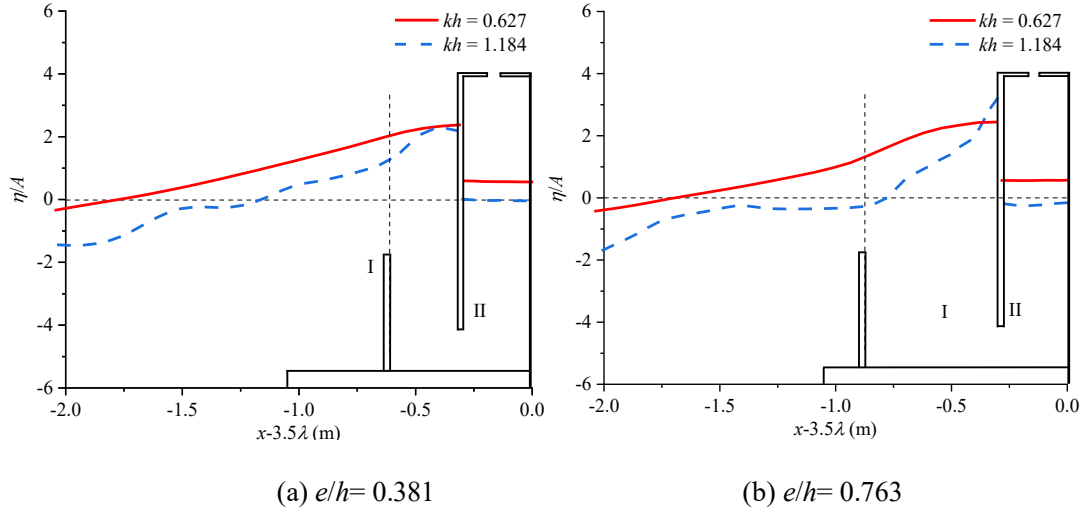(a) e/h= 0.381   (b) e/h= 0.763

Figure 14 Snapshot of free-surface elevation at the upper opening of the U-OWC device when wave crest arrives at barrier wall II for different wave frequencies.

4.3 Effect of thickness of Wall I c_I

As shown in Fig. 2, c_I denotes the thickness of barrier wall I. By setting other parameters constant as listed in Tab. 1, the effect of four thicknesses of barrier wall I of c_I/h = 0.032, 0.048, 0.064 and 0.096 on the surface-elevation amplitude η_{max} at the chamber center and the air pressure P_{max} inside the chamber are shown in Fig. 15(a) and (b), respectively. It can be seen that η_{max} and P_{max} increase with the thickness of barrier wall I increasing, but the growing trend weakens obviously with the increase of thickness. Besides, the barrier wall I thickness has little effect on the shape of the curves of the surface elevation at the chamber center and the air pressure inside the chamber. For all tested cases, η_{max} decreases with the increase of kh, and P_{max} increases initially to its peak and then decreases with kh increasing. Fig. 16 shows the effect of the barrier wall I thickness on the hydrodynamic efficiency. It can be observed that the larger thickness of barrier wall I, the higher hydrodynamic efficiency and lower resonant frequency. The optimal hydrodynamic efficiencies for c_I/h = 0.032, 0.048 0.064 and 0.096 occur at around kh =1.20, 1.17, 1.14 and 1.10 with its hydrodynamic efficiency 0.56, 0.67, 0.68 and 0.71, respectively. Additionally, similar to the trend of the surface

1 elevation and air pressure inside the chamber, the hydrodynamic efficiency also

2 increases with the thickness of barrier wall I in a declining rate. It is worth noting that

3 the construction cost increases linearly with the increase of the thickness of barrier wall

4 I. Thus, from the engineering point of view, it needs to balance the construction cost

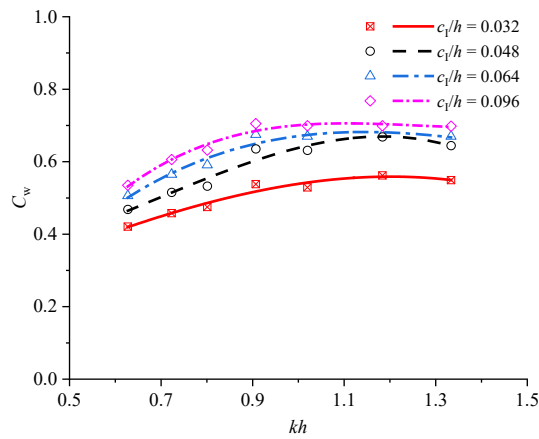5 and the hydrodynamic performance of the U-OWC device.

6

7

8 (a) Surface-elevation   (b) Air pressure
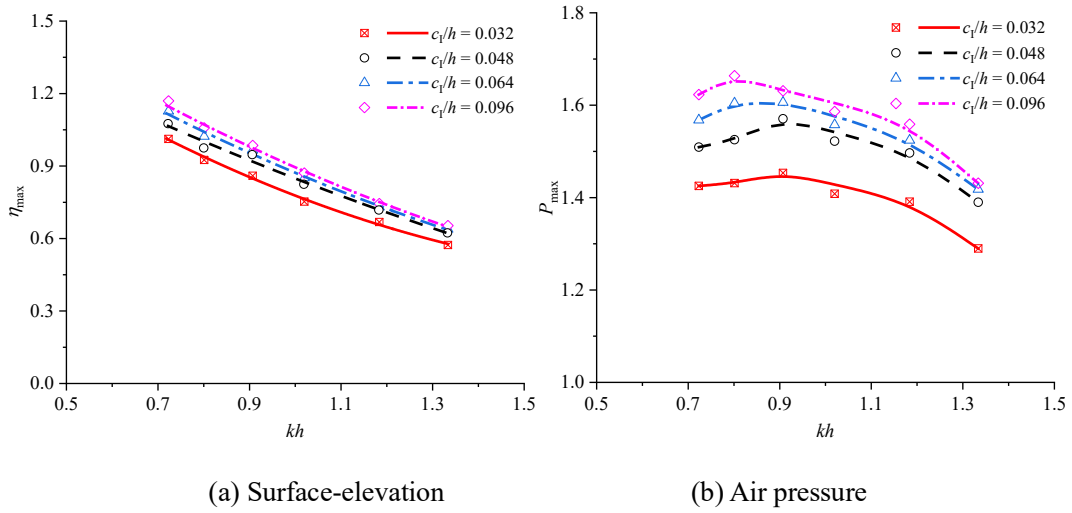
9 Figure 15 Amplitudes of the (a) surface-elevation at the chamber center and (b) air pressure inside

10   the chamber versus dimensionless wavenumber for different thicknesses of wall I.

11

12

13 Figure 16 Hydrodynamic efficiency versus dimensionless wavenumber for different thicknesses of

14   wall I.

5. Conclusions

In the present investigation, the hydrodynamic performance of the U-OWC Wave Energy Converter is analyzed. Based on the time-domain higher-order boundary element method (HOBEM), a 2-D fully nonlinear numerical wave flume with a U-OWC device is implemented to study the effects of the geometric parameters on the hydrodynamic efficiency, free-surface elevation and air pressure inside the U-OWC chamber. In the numerical simulation, the inner-source technique is used to generate incident wave to avoid re-reflection, the mixed Eulerian-Lagrangian technique and the 4th-order Runge-Kuatta method are applied as the time marching technology. The linear relationship between the air pressure inside the chamber and the air velocity at the orifice is assumed to establish the pneumatic model.

The numerical results indicate that the predicted surface elevation at the chamber center and the air pressure inside the chamber agree well with the published experimental data, generally. Further, the effects of the vertical duct height, vertical duct width and thickness of barrier wall I on hydrodynamic performance of the U-OWC device are investigated. The increase of vertical duct height can improve the hydrodynamic efficiency because the upper opening of vertical duct is closer to free surface. Therefore, the U-OWC device performs better than the conventional OWC device. As for the vertical duct width, it is observed that a larger vertical duct width leads to a larger hydrodynamic efficiency in relatively low frequency domain. However, η_{max} and P_{max} initially increase and then decrease with the increase of vertical duct width in the high frequency region. This is due to the fact that the horizontal spatial inhomogeneity of the excitation pressure at the upper opening is amplified with the decrease of wavelength (increasing wave frequency). The hydrodynamic efficiency is found to increase with the increase of thickness of barrier wall I in a declining rate. However, the construction cost increases linearly with the increase of the thickness of barrier wall I as well. Thus, from the engineering point of view, a comprehensive

consideration of the construction cost and hydrodynamic performance is necessary in the design and construction of a U-OWC device.

Acknowledgments

References

[1] A. G. L. Borthwick. Marine Renewable Energy Seascape. Engineering. 2016;2:69-78.

[2] D. V. Evans, R. Porter. Hydrodynamic characteristics of an oscillating water column device. Appl Ocean Res. 1995;15:155-64.

[3] H. Martins-rivas, C. C. Mei. Wave power extraction from an oscillating water column along a straight coast. Ocean Engineering. 2009;36:426-33.

[4] S. Zheng, A. Antonini, Y. Zhang, D. Greaves, J. Miles, G. Iglesias. Wave power extraction from multiple oscillating water columns along a straight coast. Journal of Fluid Mechanics. 2019;878:445-80.

[5] Z. Deng, L. Wang, X. Zhao, P. Wang. Wave power extraction by a nearshore oscillating water column converter with a surging lip-wall. Renewable Energy. 2020;146:662-74.

[6] D. Z. Ning, R. Q. Wang, Q. P. Zou, B. Teng. An experimental investigation of hydrodynamics of a fixed OWC Wave Energy Converter. Applied Energy. 2016;168:636-48.

[7] R.-q. Wang, D.-z. Ning. Dynamic analysis of wave action on an OWC wave energy converter under the influence of viscosity. Renewable Energy, 2020, https://doi.org/10.1016/j.renene.2020.01.007.

[8] A. F. O. Falcão, J. C. C. Henriques, J. J. Cândido. Dynamics and optimization of the OWC spar buoy wave energy converter. Renewable Energy. 2012;48:369-81.

[9] R. P. F. Gomes, J. C. C. Henriques, L. M. C. Gato, A. F. O. Falcão. Wave power extraction of a heaving floating oscillating water column in a wave channel. Renewable Energy. 2016;99:1262-75.

[10] A. J. C. Crespo, C. Altomare, J. M. Domínguez, J. González-Cao, M. Gómez-

Gesteira. Towards simulating floating offshore oscillating water column converters with Smoothed Particle Hydrodynamics. Coastal Engineering. 2017;126:11-26.

[11] F. He, Z. Huang. Hydrodynamic performance of pile-supported OWC-type structures as breakwaters: An experimental study. Ocean Engineering. 2014;88:618-26.

[12] K. Rezanejad, J. Bhattacharjee, C. Guedes Soares. Analytical and numerical study of dual-chamber oscillating water columns on stepped bottom. Renewable Energy. 2015;75:272-82.

[13] F. He, J. Leng, X. Zhao. An experimental investigation into the wave power extraction of a floating box-type breakwater with dual pneumatic chambers. Applied Ocean Research. 2017;67:21-30.

[14] D.-z. Ning, R.-q. Wang, L.-f. Chen, K. Sun. Experimental investigation of a land-based dual-chamber OWC wave energy converter. Renewable and Sustainable Energy Reviews. 2019;105:48-60.

[15] D.-z. Ning, Y. Zhou, R. Mayon, L. Johanning. Experimental investigation on the hydrodynamic performance of a cylindrical dual-chamber Oscillating Water Column device. Applied Energy. 2020;260.

[16] F. Mahnamfar, A. Altunkaynak. Comparison of numerical and experimental analyses for optimizing the geometry of OWC systems. Ocean Engineering. 2017;130:10-24.

[17] N. Dizadji, S. E. Sajadian. Modeling and optimization of the chamber of OWC system. Energy. 2011;36:2360-6.

[18] M. Kharati-Koopaee, M. Fathi-Kelestani. Assessment of oscillating water column performance: Influence of wave steepness at various chamber lengths and bottom slopes. Renewable Energy. 2020:1595-608.

[19] A. F. O. Falcão. The shoreline OWC wave power plant at the Azores,. Proceedings of the Fourth European Wave Energy Conference. Aalborg, Denmark,2000.

[20] A. F. O. Falcão, J. C. C. Henriques. Oscillating-water-column wave energy converters and air turbines: A review. Renewable Energy. 2016;85:1391-424.

[21] M. Suzuki, C. Arakawa, S. Takahashi. Performance of wave power generating system installed in breakwater at Sakata port in Japan. Proceedings of the Fourteenth International Offshore and Polar Engineering Conference. Toulon, France,May 23–28, 2004.

[22] P. Boccotti. Comparison between a U-OWC and a conventional OWC. Ocean Engineering. 2007;34:799-805.

[23] P. Boccotti. On a new wave energy absorber. Ocean Engineering. 2003;30:1191-200.

[24] P. Boccotti. Caisson breakwaters embodying an OWC with a small opening—Part I: Theory. Ocean Engineering. 2007;34:806-19.

[25] P. Boccotti, P. Filianoti, V. Fiamma, F. Arena. Caisson breakwaters embodying

an OWC with a small opening—Part II: A small-scale field experiment. Ocean Engineering. 2007;34:820-41.

[26] G. Malara, F. Arena. Analytical modelling of an U-Oscillating Water Column and performance in random waves. Renewable Energy. 2013;60:116-26.

[27] G. Malara, A. Romolo, V. Fiamma, F. Arena. On the modelling of water column oscillations in U-OWC energy harvesters. Renewable Energy. 2017;101:964-72.

[28] G. Malara, R. P. F. Gomes, F. Arena, J. C. C. Henriques, L. M. C. Gato, A. F. O. Falcão. The influence of three-dimensional effects on the performance of U-type oscillating water column wave energy harvesters. Renewable Energy. 2017;111:506-22.

[29] P. D. Spanos, F. M. Strati, G. Malara, F. Arena. An approach for non-linear stochastic analysis of U-shaped OWC wave energy converters. Probabilistic Engineering Mechanics. 2018;54:44-52.

[30] G. Malara, F. Arena. Response of U-Oscillating Water Column arrays: semi-analytical approach and numerical results. Renewable Energy. 2019;138:1152-65.

[31] F. M. Strati, G. Malara, V. Laface, A. Romolo. A Control Strategy for PTO Systems in a U-OWC Device. Proceedings of the ASME 2015 34th International Conference. Newfoundland, Canada2015.

[32] T. Vyzikas, S. Deshoulières, M. Barton, O. Giroux, D. Greaves, D. Simmonds. Experimental investigation of different geometries of fixed oscillating water column devices. Renewable Energy. 2017;104:248-58.

[33] F. Arena, L. Daniele, V. Fiamma, M. Fontana, G. Malara, G. Moretti, et al. Field Experiments on Dielectric Elastomer Generators Integrated on a U-OWC Wave Energy Converter. Volume 10: Ocean Renewable Energy2018.

[34] P. Boccotti. Design of breakwater for conversion of wave energy into electrical energy. Ocean Engineering. 2012;51:106-18.

[35] F. Arena, A. Romolo, G. Malara. On Design and Building of a U-OWC Wave Energy Converter in the Mediterranean Sea: A Case Study. Proceedings of the ASME 2013 32nd International Conference. Nantes, France2013.

[36] D. Z. Ning, J. Shi, Q. P. Zou, B. Teng. Investigation of hydrodynamic performance of an OWC (oscillating water column) wave energy device using a fully nonlinear HOBEM (higher-order boundary element method). Energy. 2015;83:177-88.

[37] R. Q. Wang, D. Z. Ning, C. W. Zhang, Q. P. Zou, Z. Liu. Nonlinear and viscous effects on the hydrodynamic performance of a fixed OWC wave energy converter. Coastal Engineering. 2018;131:42-50.

[38] W. Koo, M. H. Kim, D. H. Lee. Nonlinear Time-domain Simulation of Pneumatic Floating Breakwater. International Journal of Offshore and Polar Engineering. 2006;16:25-32.